Petroleum Science 18 (2021) 1357–1369

Contents lists available at ScienceDirect

Petroleum Science

journal homepage: www.keaipublishing.com/en/journals/petroleum-science

Original Paper

3D geo-cellular static virtual outcrop model and its implications for reservoir petro-physical characteristics and heterogeneities

Muhammad Usman [a, b], Numair A. Siddiqui [b], Shi-Qi Zhang [a, *], Manoj J. Mathew [c], Ya-Xuan Zhang [d], Muhammad Jamil [b], Xue-Liang Liu [e], Nisar Ahmed [b]

[a] School of Geosciences, China University of Petroleum (East China), Qingdao, 266580, Shandong, China
[b] Department of Geosciences, Universiti Teknologi PETRONAS, Bandar Seri Iskandar, Perak, Malaysia
[c] Laboratoire Géosciences Océan, IUEM, Université de Brest, UMR 6538 CNRS/UBO/UBS, RueDumont D'Urville, 29280, Plouzané, France
[d] School of Geosciences, The University of Edinburgh, Edinburgh, UK
[e] Lukeqin Oil Producion Plant, PetroChina Tuha Oilfield, Shanshan, 838202, Xinjiang, China

ARTICLE INFO

Article history:
Received 27 July 2020
Accepted 5 March 2021
Available online 11 September 2021

Edited by Jie Hao

Keywords:
Virtual outcrop modeling
Lithofacies
3D geo-cellular model
Petrophysical properties
Reservoir heterogeneities

ABSTRACT

Geostatistical data plays a vibrant role for surface-based reservoir modeling through outcrop analogues, which is used to understand three-dimensional (3D) variability of petrophysical properties. The main purpose of this study is to improvise the surface-based 3D geo-modeling to demonstrate petrophysical characteristics and heterogeneities of Sandakan reservoirs, NW Borneo. We used point cloud data from Light Detection and Ranging (LiDAR) to build high-resolution virtual outcrop modeling (VOM) onto which we mapped 6 different lithofacies. Porosity and permeability of core plugs were measured to determine the average variance of petrophysical properties for each lithofacies. By utilizing the integration of VOMs analogues and petrophysical properties in Petrel™, we demonstrated the distribution and associations of all lithofacies in pseudo wells that have inherent thin beds heterogeneities in 3D geo-cellular model. The results concluded that the heterogeneity of thin beds in lithofacies is dependent on porosity and permeability with input dataset. According to the final model, cross-bedding sandstone (CBS), hummocky cross-stratified sandstone (HCSS) and trough cross-bedding sandstone (TCBS) show good reservoir quality due to high porosity ranging from: 25.6% to 20.4% and, 19.3%–14.5%, and permeability ranging from: 74.03 mD to 66.84 mD and, 64.86 mD to 21.01 mD. In contrast, massive to weak laminae sandstone (MWLS) and bioturbated sandstone (BS) show fair to poor reservoir quality, caused baffling of surrounding mud sediments in the reservoir lithofacies. Results also revealed that LiDAR based VOM with petrophysical properties can significantly reduce the risk and minimize the cost of reservoir modeling in petroleum industry.

1. Introduction

Outcrop analogues set forth in the form of geostatistical and high resolution 2D or 3D digital records that effectively help to handle the large scale reservoir modeling challenges (Jackson et al., 2005; Enge et al., 2007; Jones et al., 2008; Howell et al., 2014; Wilkinson et al., 2016), such as, the understanding of heterogeneity in geo-cellular and petrophysical modeling of subsurface reservoirs to enhance the quantitative spatial accuracy (Tinker, 1996; Bryant et al., 2000; Fabuel-Perez et al., 2009b; 2010; Rarity et al., 2014; Wilkinson et al., 2016). The geo-cellular modeling is 3D volume of the reservoir media that includes 3D cells meshes with complete illustration of stratigraphic packet, reservoir sublayers/horizons and faults (Shepherd, 2009; Yarus et al., 2012; Fei et al., 2016; Gomes et al., 2018; Usman et al., 2021). More recently, the geo-cellular modeling of different lithofacies from outcrop analogues has been widely applied to the fluvial braided systems based on subsurface data (Pringle et al., 2006; Howell et al., 2014), but petrophysical heterogeneity in the thin beds remains unsolved through surface data. Conventionally, seismic, well logs, and petrophysical datasets are useful for reservoir and petrophysical modeling (Henriquez and Jourdan, 1995; Charles, 1999;

* Corresponding author.
E-mail address: shqzhang@upc.edu.cn (S.-Q. Zhang).

https://doi.org/10.1016/j.petsci.2021.09.021

Brandsæ;ter et al., 2005) but limited to spatial variations and thin beds resolution in the reservoir media (Rarity et al., 2014). Regarding this, the digital scanning of outcrop analogues plays a dynamic protagonist in the examination of reservoir heterogeneities with petrophysical modeling in thin bedded media (Fabuel-Perez et al., 2010; Pavlis and Bruhn, 2011; Pavlis and Mason, 2017). The digital scanning of outcrops through LiDAR provides quantitative data (e.g., point clouds, photorealistic 3D models, and measurements with orientations, polylines) for the lithofacies (geobodies) modeling (Notebaert et al., 2009; Fabuel-Perez et al., 2009b; 2010) to demonstrate the heterogeneity with spatial and temporal variations of petro-physical data (Immenhauser et al., 2004; Mikes and Geel, 2006; Jones et al., 2008a; Amour et al., 2012).

Acquisition of the outcrop analogues is usually performed through scanning techniques, such as the Light Detection and Ranging (LiDAR) (Xu et al., 2000; Slob and Hack, 2004; Bellian et al., 2005; Bellian et al., 2007; Siddiqui et al., 2019), which acquires outcrop dataset in the form of point clouds and photorealistic 3D models for virtual outcrop modeling (VOM) (Enge et al., 2007; Pranter et al., 2007; Buckley et al., 2008; Jones et al., 2008; Fabuel-Perez et al., 2010) and structure from motion (SFM) algorithm for the high resolution 3D terrain models (Westoby et al., 2012; Wilkinson et al., 2016; Brush et al., 2019). The VOM analogues are used for the stochastic facies modeling to document the dimensions and geometry of lithofacies in the surface and subsurface reservoirs (Coburn et al., 2006) to enhance the resolution of the geo-cellular modeling for thin bedded reservoir media to understand its reservoir heterogeneity at micro to mesoscale (Jackson et al., 2005; Coburn et al., 2006; Siddiqui et al., 2019). In outcrop-based modeling, the lateral and vertical extensions of sedimentary lithofacies in every horizon have primary controls on flow simulation (Fabuel-Perez et al., 2009b; 2010; Siddiqui et al., 2019). This shows that the flow simulation in reservoir modeling depends on the qualitative and quantitative datasets in the VOM to elucidate the petrophysical heterogeneities of lithofacies (Kjønsvik et al., 1994; Løseth et al., 2004; Adams et al., 2005; Falivene et al., 2006b; Eaton, 2006; Aigner et al., 2007; Qi et al., 2007; Phelps et al., 2008; Verwer et al., 2009; Palermo et al., 2010; Tomàs et al., 2010; Amour et al., 2012; Wilkinson et al., 2016). Whereas, for dynamic flow simulation in reservoir modeling, algorithms that are supportive in stochastic lithofacies are applied to different reservoir settings e.g., in channel-fill turbidites (Falivene et al., 2006b). These algorithms including Truncated Gaussian Simulation (TGSim), Sequential Indicator Simulation (SISim) and Indicator Kriging (IK) (White et al., 2003; Zappa et al., 2006; Aigner et al., 2007; Falivene et al., 2007; Tolosana-Delgado et al., 2008; Koehrer et al., 2010), are implanted in the reservoir modeling software (i.e., Petrel™ Suite) and provide a variety of simulated models (Gotway and Rutherford, 1994; Bastante et al., 2008).

In this study, we have used Sequential Indicator Simulation (SISim) algorithm that is useful and sensitive to elucidate the 3D geo-modeling of thin bedded reservoirs. In the Sabah, northwest Borneo, subsurface Neogene sedimentary rocks have significant interests for hydrocarbon (HC) exploration because same age rocks have been producing HC offshore in the West Borneo (Sarawak) (Fig. 1) (Madon, 1999; Siddiqui et al., 2020). Different researchers have already done intensive reservoir sedimentological research in the Sabah (Lee, 1970; Graves and Swauger, 1997; Hutchison, 2005; Futalan et al., 2012, Menier et al., 2017; Siddiqui et al., 2019, 2020; Usman et al., 2020a, b, c) but have not yet any avenues for 3D geo-modeling to demonstrate the spatial and temporal heterogeneity in the siliciclastic rock types for reservoir study. The main purpose of this study is to elaborate the integrated studies of reservoir in the 3D geo-cellular modeling based on outcrop analogues through LiDAR for VOM to demonstrate the petrophysical and heterogenetic characteristics of well exposed reservoir rocks of Sandakan Formation, NW, Borneo (**Fig. 1**). All input datasets for the interpretation of lithofacies, their horizons, pseudo wells in the Virtual Reality Geological Studio (VRGS) and an industrial reservoir modeling software (Petrel™ Suite) were collected through conventional fieldwork and LiDAR scanning and data processing of different sections in northwest Borneo formation (**Fig. 1a**). The workflow and results of this study are useful to understand subsurface reservoir models and 3D geometry, to elucidate the thin bedded reservoirs conditions that are difficult to recognize using seismic and geophysical well log datasets.

2. Geological setting

Borneo was formed with complex tectonic processes due to the collision of micro continental fragments with the Paleozoic part of Sunda Plate (Mathew et al., 2014a, Mathew et al., 2016; Ramkumar et al., 2018; Usman et al., 2020a). Northwest Borneo mainly comprises of Sarawak and Sabah Basins that is a large orogenic belt along the continental margin of the South China Sea (Rangin et al., 1990; Siddiqui et al., 2019, 2020; Usman et al., 2020) (Fig. 1a). The Sabah Basin experienced very complex tectonic history that had been discussed by many researchers (e.g., Madon, 1999; Hall, 2002; Hutchison, 2005; Sapin et al., 2011; Hall, 2013; Franke et al., 2014; Mathew et al., 2016, Usman et al., 2020a, Ahmed et al., 2021a, b; Jamil et al., 2020). The basin is mainly filled up with Neogene sediments with intense tectonic history including Late Miocene Sandakan Formation (Fig. 1a) (Mathew et al., 2016a, Mathew et al., 2016b, Menier et al., 2017; Usman et al., 2020a). North East Sabah Basin has two parts i.e., central Sabah sub-basin and Sandakan sub-basin (Bell and Jessop, 1974; Tjia et al., 1990; Siddiqui et al., 2019; Siddiqui et al., 2020; Usman et al., 2020a, c). Sandakan sub-basin is a Peninsula of east Sabah, northwest Borneo that is bounded between longitudes 117° 90' E and 118° 10' E and latitudes 5° 75' N and 6° 00' N (Fig. 1b). The Sandakan sub-basin mainly consists of Upper Miocene rocks that were deposited within a circular basin with multiple sediment sources (Clennell, 1996) and in the shallow marine trough (Collenette, 1965a; 1966). Primary sedimentary structures such as crossbedding, current and wave ripples, channeling and hummocky with bioturbation (Siddiqui et al., 2019, 2020; Usman et al., 2020a, c) are very common. The Sandakan Formation unconformably overlies by Quaternary deposits (Fig. 1b),and in onshore area it can be correlated with Bongaya Formation (Wilson, 1961; Lee, 1970). The Sandakan Formation mainly consists of Late Miocene sandstone, mudstone with the amalgamation of siltstone and coal lamina, and its thickness has been reported almost 2500 m (Fig. 1b) (Azlina and Muhammad, 1995; Siddiqui et al., 2019, 2020; Usman et al., 2020a, c). It is overlain unconformably by Quaternary deposits and can be correlated with Bongaya Formation in onshore area (Wilson, 1961; Lee, 1970). Based on primary sedimentary structures and ichnofacies in the muddy-sandstone and mudstone, researchers (Lee, 1970, Stauffer and Lee, 1972, Usman et al., 2020a, b, c) suggested that it has fluvial source and mainly deposited in shallow marine as Late Miocene. In the past, there have been many hydrocarbon discoveries in the Early-middle Miocene sandstone of the northeast Sabah Basin, including offshore Sandakan sub-Basin (Madon, 1999), coeval sandstone of Sandakan Formation in the onshore area shows good reservoir potential (Azlina and Muhammad, 1995).

3. Methodology and workflow

3.1. Fieldwork for sedimentological architecture and core plugs

Four (4) well-exposed outcrop sections to the northwest part of

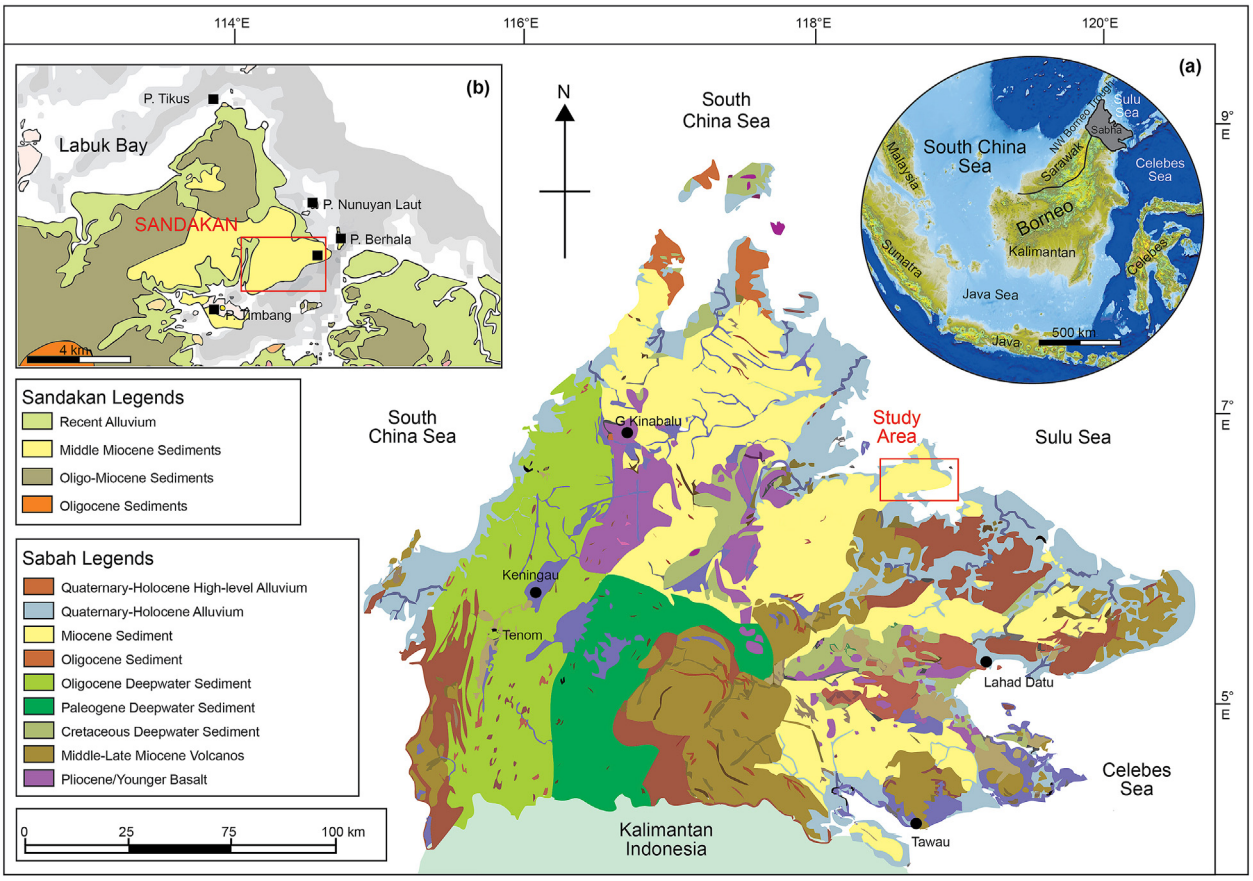

Fig. 1. Geologic maps. (a) NW, Borneo that is Sarawak and Sabah Basin and consists of Quaternary sediments to ophiolitic and igneous rocks with the close-up view in the main figure for the understanding of deposited sediments. (b) shows the close-up view of the Miocene sediments in the study area of the Sandakan Formation, NW, Borneo (Modified after Usman et al., 2020a, c).

Borneo (Fig. 1a) were chosen for field based sedimentological architecture study, and thirty (30) core plugs were plugged out from these sections with handheld coring machine. For sedimentological architecture, we measured the thickness of the sections with grain size variations and recorded primary sedimentary structures and borrowing index. Following facies scheme of Siddique et al. 2019, we marked six (6) outcrop lithofacies of Sandakan Formation for further 3D geo-cellular and geo-modeling studies. Porosity and permeability of all recovered core plugs from these lithofacies were analyzed using Helium Porosimeter and Helium Poroperm to document the petro-physical heterogeneity in the geo-cellular model with pseudo wells using reservoir modeling software Petrel™ Suite (Fig. 2).

3.2. Methodology: Creation of Virtual Outcrop Modeling (VOM)

Well-exposed outcrops with lateral and vertical extensions are good representatives for reservoir modeling (Arbués et al., 2007; Fabuel-Perez et al., 2009b; 2010). Digital scanning techniques have been developed to construct high-resolution outcrop analogues for better understanding of reservoirs (Pringle et al., 2006; Enge et al., 2007; Gold et al., 2012). We used RIEGL VZ-2000i long range 3D Light detection and ranging (LiDAR) laser scanner of LMS-Z series to acquire the point cloud dataset with 3D photorealists images from the four outcrops of the Sandakan Formation, northwest Borneo for virtual reality modeling (VRM). LiDAR was chosen for its effectiveness in mapping and digitization (Gold et al., 2012; Buckley et al., 2016; De Paor, 2016) in the regions with very thick vegetation and/or difficult to access for the three-dimensional (3D) outcrops modeling. For the virtual outcrop modeling (VOM), the LiDAR dataset consists of field data and digital scanning data of the measured sections with dGPS points and scanned photographs with maximum ranging of the features. The sedimentological features including sedimentary structures with paleocurrent measurements and lithofacies with the variations of grain size were recorded in the form of logs. Both sedimentological and LiDAR data further were used in Virtual Reality Geological Studio (VRGS) to interpret and digitize the identified lithofacies within stratigraphic horizon framework, and then were processed to make the VOMs for further interpretation and modeling.

3.2.1. Data acquisition and processing

Details of collecting and processing of point cloud dataset of the LiDAR have been described by many researchers (i.e., Pringle et al., 2006; Bellian et al., 2005; Enge et al., 2007; Buckley et al., 2008; Kurz et al., 2011; Gold et al., 2012; Sima, 2013, Howell et al., 2014; Siddiqui et al., 2019) for reservoir modeling. The acquired data from LiDAR (Siddiqui et al., 2019) was then re-processed by using RiScan Pro v2.1.1 software according to the Fabuel-Perez et al. (2010) for the 10,000 points/second that were interdepended on the rock reflectivity and weathering with ±0.01 mm accuracy.

3.2.1.1. ***Pre-processing of dataset***. The LiDAR Point-cloud data were acquired with 8-scan positioning on the 250 m^2 thick succession of the Sandakan Formation, northwest Borneo. The data contain ≥210 million points in *x, y, z* format that based on outcrop

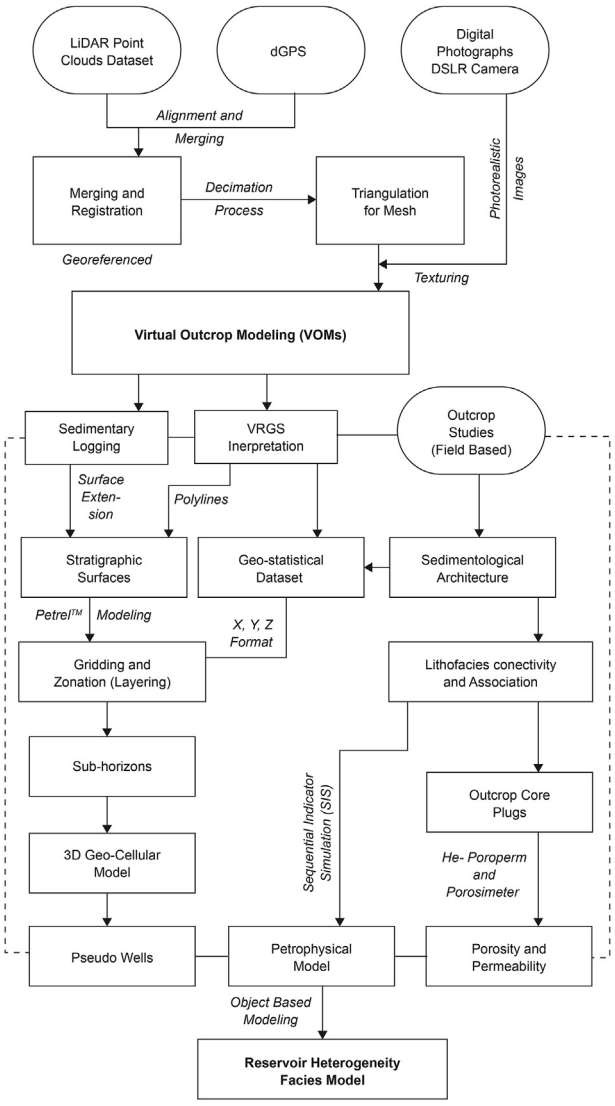

Fig. 2. Complete workflow used for the Creation of Virtual Outcrop Modeling (VOM) and 3D geo-model based on LiDAR input dataset. Rounded box shows the mainly used input dataset and italic text shows processes which are used for getting the final 3D reservoir heterogeneity facies model (modified after Fabuel-Perez et al., 2010; Siddiqui et al., 2019).

reflectivity and distance between outcrop and scanning laser. These scan positions contain 360° low resolution panoramic view, and the high-resolution scan view of the interested area was prepossessed by using the RiScan Pro software. The high-resolution scan views were resized at 0.01 mm from a very large dataset (≥20 GB) that were at 0.004 mm point cloud spacing in order to handle the dataset easily. The acquired scan photographs from the mounted and calibrated DSLR Nikon Camera (12 megapixels) covers the entire outcrop. Merging process and registration of different scan positions were completed by picking points manually using transformation matrix of the RiScan Pro v2.1.10 software with the Global Cartesian Coordinate System.

3.2.1.2. ***Post-processing***. DGPS information was used to provide the globally correct scanning positions according to UTM (Universal Transverse Mercator) coordinate system in the pre-processed dataset. All vegetations and noises were removed by using the Object Manager and Echo options for further processing. The cleaned scans were triangulated to get the mesh file on which 3D photorealistic images of panoramic views were dressed up. To reduce the numbers of triangles in the mesh file, the mesh decimation process was subjected without changing of geometry and shape of the final model (Fig. 2). In the end, to get the original color of scans each vertex was mapped in the mesh back that was textured with digital images. Each pixel in 3D photorealistic images of panoramic view was related to *x, y, z* coordinates with corrected triangular vertex. This process was done on the three sections of the study area to gain the resultant virtual outcrop modeling (VOM) model.

3.3. Generation of geo-cellular and petrophysical modeling (geo-modeling)

VOM analogues were used as input dataset for the geo-cellular modeling that is a 3D gridding volume of the reservoir media with the complete illustration of stratigraphic strata interval, reservoir sublayers/horizons and faults in the form of 3D cells meshes (Shepherd, 2009; Yarus et al., 2012; Fei et al., 2016; Gomes et al., 2018). The analogue based geo-modeling can be improved by increasing the resolution and removing of the uncertainties (Jackson et al., 2005; Coburn et al., 2006; Fabuel-Perez et al., 2009b; 2010; Siddiqui et al., 2019). The required dataset for high resolution reservoir with limited uncertainties for 3D geo-cellular gridding and geo-modeling can be seen in detail from Fabuel-Perez et al. (2009b, 2010). The recommended dataset is used for 3D geo-modeling of lithofacies with the help of marked horizons that extracted from the processed VRGS and interpreted on VOMs (Figs. 2 and 3). The extracted VOMs data (horizons and dGPS analogue data) from the marked VRGS lithofacies were imported into the Petrel™ Suite for the further interpretations, 3-D modeling, and flow stochastic simulation (Fig. 3). The geo-modeling of the reservoir is very helpful to understand and visualize the subsurface events, reservoir property and its petrophysical heterogeneity (Bryant et al., 2000; Fabuel-Perez et al., 2009b, 2010; Rarity et al., 2014).

3.3.1. Pseudo wells

Field based sedimentary logs were interpreted in VRGS software to make the pseudo wells for digital lithology, grain size, thickness, sedimentary structures and paleocurrent directions with the accurate coordinates. This georeferenced sedimentary logs data was imported into the Petrel™ (Fabuel-Perez et al., 2010; Rarity et al., 2014) as pseudo wells in *x, y, z* format to generate the horizons and sub-horizons. The pseudo wells data is used to improve the sedimentological details in lithofacies modeling, to confirm the geo-cellular modeling with respect to horizons and sub-horizons and also to control the qualitative measurements of the geo-cellular model. Four pseudo wells with all interpreted properties of measured sections with vertically thickness were imported into the Petrel™ Suite.

3.3.2. Interpretation of key horizons (stratigraphic surfaces) and generation of sub-horizons (layering)

Key horizon interpretation of pseudo wells was completed by importing the VOMs data that were interpreted and generated by the LiDAR georeferenced data (Bryant et al., 2000; Fabuel-Perez et al., 2010; Rarity et al., 2014) into the VRGS in *x, y, z* format. It is challenging to generate the 3D key surfaces that are needed to show the geo-cellular area of the reservoir (Enge et al., 2007; Buckley et al., 2008; Fabuel-Perez et al., 2010; Rarity et al., 2014). Five horizons in the VRGS were generated based on the marked lithofacies using triangulated irregular network (TIN) algorithm of VOMs sections according to Fabuel-Perez et al. (2010) and Rarity

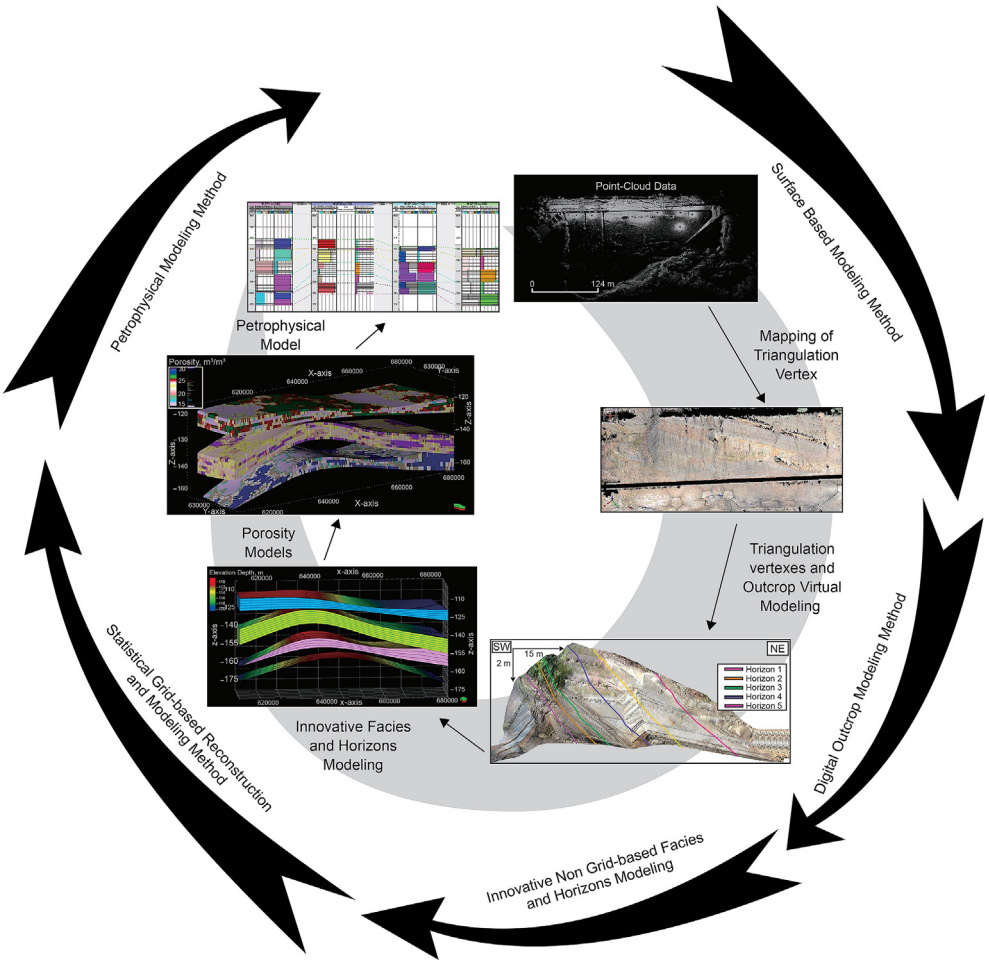

Fig. 3. Complete workflow from surface-based virtual outcrop modeling (VOM) to pseudo wells petrophysical modeling of stochastic lithofacies. This workflow includes input dataset of VOMs, pseudo well, interpretation of key horizons with sub-horizons, 3D geo-cellular gridding and petrophysical models lithofacies.

et al. (2014). TIN surface in VRGS is the combined algorithm study of the interpreted lithofacies with their dip and strike that is helpful for horizontal extrapolation of the original data in the Petrel™, although uncertainties are also high due to extrapolation (Redfern et al., 2007; Wilson et al., 2009; Fabuel-Perez et al., 2010). The extrapolated data may be varied from its original positions (Redfern et al., 2007) but maintain original thickness that shows the key horizons. Then it was further used in the 3D Stochastic model for the petrophysical simulation with the generation of sub-horizons according to the thickness of the marked lithofacies in the field study. The outcrop analogue is one of the best measured tools, which is used in the reservoir modeling to observe the heterogeneity in all surfaces and subsurface of lithofacies in 3D geo-cellular model.

3.4. 3-D geo-cellular modeling and lithofacies gridding

Gridding is the first step to generate the 3D geo-cellular model of lithofacies. We used stratigraphic surfaces and sub-horizons (layering) in the geo-cellular model to build 3-D lithofacies gridding in the Petrel™ Suite. To make it more realistic, we used corner coordinates of the VOMs outcrop model and porosity and permeability for the petrophysical model. The geo-cellular model covers the three dimensional (3D) large area in *X, Y* and *Z* directions (Fabuel-Perez et al., 2010; Howell et al., 2014). *X* and *Y* directions show the heterogeneities in the reservoir media and *Z* direction shows the vertical resolution that was extrapolated in the modeling software for higher resolution and better studies to know the temporal and spatial variations in lithofacies model. The pseudo wells were used for geo-cellular modeling of the lithofacies which was defined in the *X* and *Y* dimensions of the gridding according to our study area to represent the lithofacies associations.

3.5. Stochastic modeling: petrophysical modeling

Stochastic modeling is based on three types of simulation algorithms: Truncated Gaussian Simulation (TGSim), Sequential Indicator Simulation (SISim), and Indicator Kriging (IK) in the reservoir modeling Petrel™ software for different models with same datasets (Gotway and Rutherford, 1994; Bastante et al., 2008). In this study, SISim has been used for 3D lithofacies, and high-resolution subsurface thinly bedded reservoir in terms of petrophysical heterogeneities in the reservoir model. Upscaling of the pseudo wells with the SISim was done according to the lithofacies thickness to mark sub-horizons in the key horizon of same facies for high resolution of heterogeneity in geo-cellular model.

4. Results

4.1. Architecture and lithofacies associations

Based on sedimentary structures, texture, and grain size, six

lithofacies types (Fig. 4) of Sandakan Formation were recognized to the following scheme of Siddiqui et al. (2019). Measured porosity and permeability by Helium poroperm and porosimeter through outcrop core plugs in the laboratory have been assigned to each lithofacies.

i **Parallel Laminated Sandstone (PLS)**

PLS consists of white to pale light yellow parallel laminated, fine to medium grained well sorted sandstone and has sharp contact with mudstone (Fig. 4a). In the measured section, PLS is mostly associated with the planar cross-bedded and massive sandstone facies. PLS lithofacies formed by the rapid influx of sediments with interbedded slow deposition of mud layers (Fig. 4a). PLS porosity and permeability ranges are 27.0%–20.2% and 12.83 mD to 9.08 mD, respectively (Table 1).

ii **Bioturbated sandstone (BS)**

BS consists of the grey to light grey fine to very fine grained and well sorted sandstone. There is sharp contact between massive sandstone beds and mudstone at the bottom of BS (Fig. 4b). BS is associated with low angle hummocky and massive sandstone facies. It has been deposited by the high storm reworking sediments (Fig. 4b). There are three predominantly ichnofacies that are *Psilonichnus, Skolithos, and Cruziana* with dense ichnofabrics in the measured section. Porosity and permeability range in the BS vary from 18.61% to 21.01% and 19.10 mD to 15.73 mD, respectively (Table 1).

iii **Cross-Bedded Sandstone (CBS)**

CBS consists of light grey, poorly sorted, fine-grained sandstone with some mud drapes and coal layers (Fig. 4c). Low angle cross-bedded and planar bedding is very common in the measured sections. CBS facies were formed by the downstream migration of bed forms and laterally continuing within the whole beds of the Sandakan Formation and lamination at the base of CBS is nearly parallel (Fig. 4c). Its porosity and permeability range from 25.6% to 15.5% and 74.03 mD to 66.84 mD, respectively (Table 1).

iv **Trough Cross-Bedded sandstone (TCBS)**

TCBS is yellowish color, trough shaped, fine grained, moderately to well sorted sandstone. Its trough crossbedding cut or overlap each other with coal clasts, mixed mud-clasts, and mud-drapes. TCBS formed in the tide dominated migration of sinuous crested and associated with the MS, BS, and PLS lithofacies (Fig. 4d). Porosity and permeability of TCBS range vary from 19.3% to 17.6% and 64.86 mD to 21.01 mD, respectively (Table 1).

v **Hummocky Cross-Stratified Sandstone (HCSS)**

HCSS consists of very light-yellow, well sorted, fine to medium grained sandstone with an erosive base and a sharp top bounded by mudstone (Fig. 4e). HCSS shows low angle lamina and are associated with the TCBS, BS, and PLS lithofacies. Bioturbation is present within this facie in the measured sections. HCSS was formed during the storm wave through reworking previously deposited sediments (Fig. 4e). Porosity and permeability range vary from 14.5% to 15.5% and 69.86 mD to 65.76 mD, respectively (Table 1).

vi **Massive to Weak Laminae Sandstone (MWLS)**

MWLS consists of light yellow, fine to medium grained, well sorted sandstone with weak parallel or horizontal lamina (Fig. 4f), which is restricted to the discrete patches that are not present throughout the lithofacies. MWLS deposited by the rapid

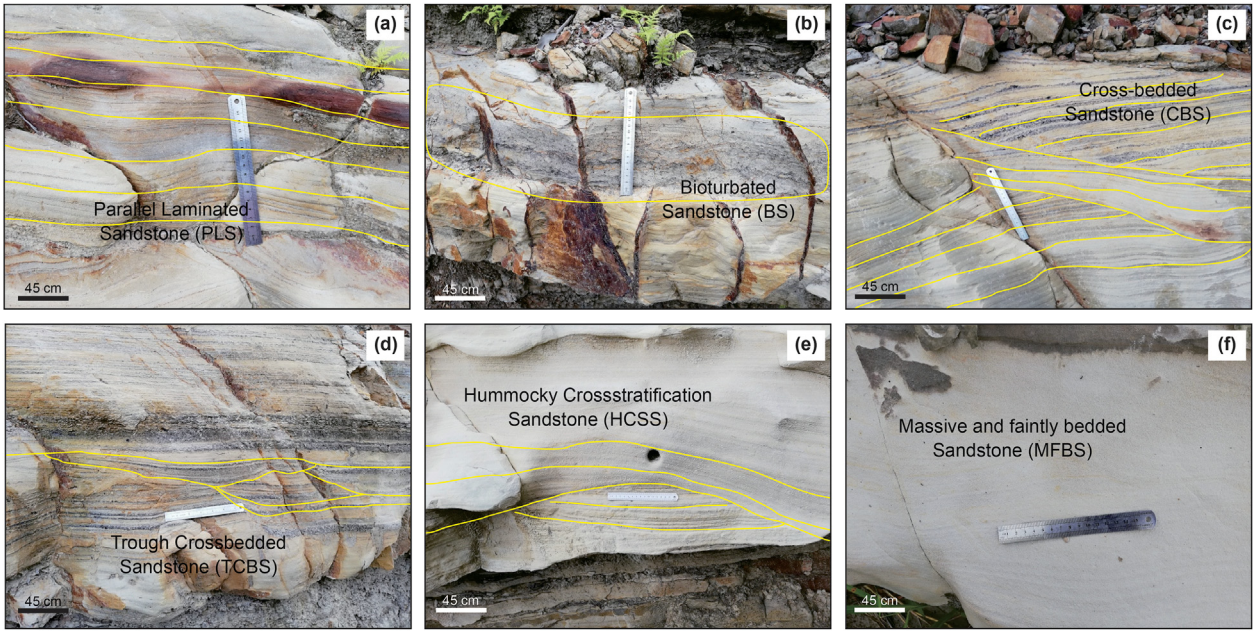

Fig. 4. Six (6) marked lithofacies on the outcrop sections with the interpretation of the primary sedimentary structures in yellow color lines. (a) shows the parallel laminated sandstone (PLS) which is mostly associated with planar cross-bedded and massive sandstone facies. (b) shows the dense bioturbated sandstone (BS) facies which is mostly associated with low angle hummocky and massive sandstone. (c) shows the cross-bedded sandstone (CBS) with low angle cross-bedded and planar bedding. (d) shows the trough cross-bedded sandstone with MS, BS, and PLS lithofacies. (e) shows the hummocky cross-stratified sandstone (HCSS) with TCBS, BS, PLS lithofacies. (f) shows the massive to weakly laminae sandstone (MWLS) which is mostly associated with LCS and PLS lithofacies.

Table 1
Shows the lithofacies heterogeneity respective to their measured thickness scales with porosity and permeability.

Details of the Lithofacies Heterogeneity (Interpreted DVOMs in the VRGS)							
Harbuor View							
Labels	Lithofacies Code	Lithofacies	Thickness (m)	Grain Size	Sedimentary Structures	Porosity (%)	Permeability (mD)
a	PLS	Parallel Laminated Sandstone	6	Medium Coarse	Planar and Laminated	20.2	9.08
b	CBS	Cross-Bedded Sandstone	6	Coarse	Cross-Lamination and Stratification	15.5	65.76
c	MFBS	Massive and Weakly Bedded Sandstone	24	Very Coarse	Structureless with Weakly Planar Lamination	16.7	66.84
d	BS	Bioturbated Sandstone	13	Coarse	Fills with Surrounding Sediments	21.0	15.73
e	TCBS	Trough Cross-Bedded Sandstone	15	Very Coarse	Trough Cross Stratification	19.3	64.86
m	M	Mudstone	17	Very Fine	Structureless	–	–
Ulu Sibuga							
Labels	Lithofacies Code	Lithofacies	Thickness (m)	Grain Size	Sedimentary Structures	Porosity (%)	Permeability (mD)
m	M	Mudstone	27	Very Fine	Structureless	–	–
a	CBS	Cross-Bedded Sandstone	5	Medium Coarse	Cross-Lamination and Stratification	16.9	66.84
b	WS	Wavy Sandstone	8	Coarse	Wavy and Rippling	20.2	96.92
c	HCSS	Hummocky Cross-Stratified Sandstone	5	Medium Coarse	Hummocky Cross Stratification	14.5	69.86
d	MFBS	Massive and Weakly Bedded Sandstone	21	Coarse	Structureless with Weakly Planar Lamination	17.3	63.67
m	M	Mudstone	27	Very Fine	Structureless	–	–
Taman Malanta							
Labels	Lithofacies Code	Lithofacies	Thickness (m)	Grain Size	Sedimentary Structures	Porosity (%)	Permeability (mD)
a	PLS	Parallel Laminated Sandstone	25	Fine	Planar and Laminated	27.0	12.83
b	BS	Bioturbated Sandstone	11	Coarse	Fills with Surrounding Sediments	18.6	19.10
c	CBS	Cross-Bedded Sandstone	8	Medium Coarse	Cross-Lamination and Stratification	25.6	74.03
d	HCSS	Hummocky Cross-Stratified Sandstone	5	Medium Coarse	Hummocky Cross Stratification	15.5	65.76
e	TCBS	Trough Cross-Bedded Sandstone	22	Medium Coarse	Trough Cross Stratification	17.6	21.01
f	MFBS	Massive and Weakly Bedded Sandstone	33	Coarse	Structureless with Weakly Planar Lamination	20.0	81.52

deposition or by the sediment gravity flow associated with LCS and PLS lithofacies (Fig. 4f). Its porosity and permeability range from 20.0% to 16.7% and 81.52 mD to 63.67 mD, respectively (Table 1).

4.2. LiDAR and VRGS based virtual outcrop modeling (VOM)

Three (3) out of four (4) well-exposed outcrops sections were selected for the LiDAR scanning. The acquired data in the form of thousands of point clouds were processed in the RiScan Pro software to get the textural digital model. Digital triangulated meshed model of outcrop in the form of virtual outcrop modeling (VOM) (Fig. 5) was built from RiScan Pro software after all processing steps (see details in section 3.2). To interpret the sedimentological parameterization of the outcrops, the high-resolution digital model from RiScan Pro was imported into the Virtual Reality Geological Studio (VRGS) software in the form of LAS file. Analogues of sedimentological parameterization of architectural studies are (Fig. 5): (1) sedimentological logs, including grain size, lithology, bed thickness, facies association and sedimentary structures; and (2) building horizons and digitizing according to the marked lithofacies of the Sandakan Formation. These analogues are the substitutions as the subsurface dataset, which has been discussed in section 4.4 for the geo-modeling of the lithofacies.

4.3. Input data integration as pseudo wells for 3D geo-modeling and quantitative analysis

Integration of scanned and digital dataset is very important for the 3D geo-modeling analysis through geo-cellular and petrophysical models (Pringle et al., 2006). The input dataset includes a suite of 1D georeferenced outcrop sections and well logs, photorealists images, horizons interpretations, dGPS dataset, point cloud data with textured surfaces through LiDAR and RiScan Pro as VOMs and geophysical dataset. The obtained virtual models were then manually interpreted to show the actual and real field-based facies variations (Fig. 5), association and their thickness from the lateral connectivity of sedimentary logs (Fig. 6) as an input dataset for modeling. In addition, sedimentological parameterization including facies distribution (Fig. 6), bedding features (dip, strike, paleocurrent flow direction) were extracted from pseudo wells and field photographs of Siddiqui et al. (2019). The input dataset as; georeferenced sedimentary logs (pseudo wells), point sets (*X, Y, Z* format) of interpreted horizons imported into the Petrel™ software to obtain spatial models. Reservoir 2D connectivity in the lithofacies and uncertainties in 2D flow simulation model were estimated from Siddiqui et al. (2019). All obtained datasets from VOMs and photorealistic images with sedimentological studies, horizons and pseudo wells were populated in the Petrel™ according to

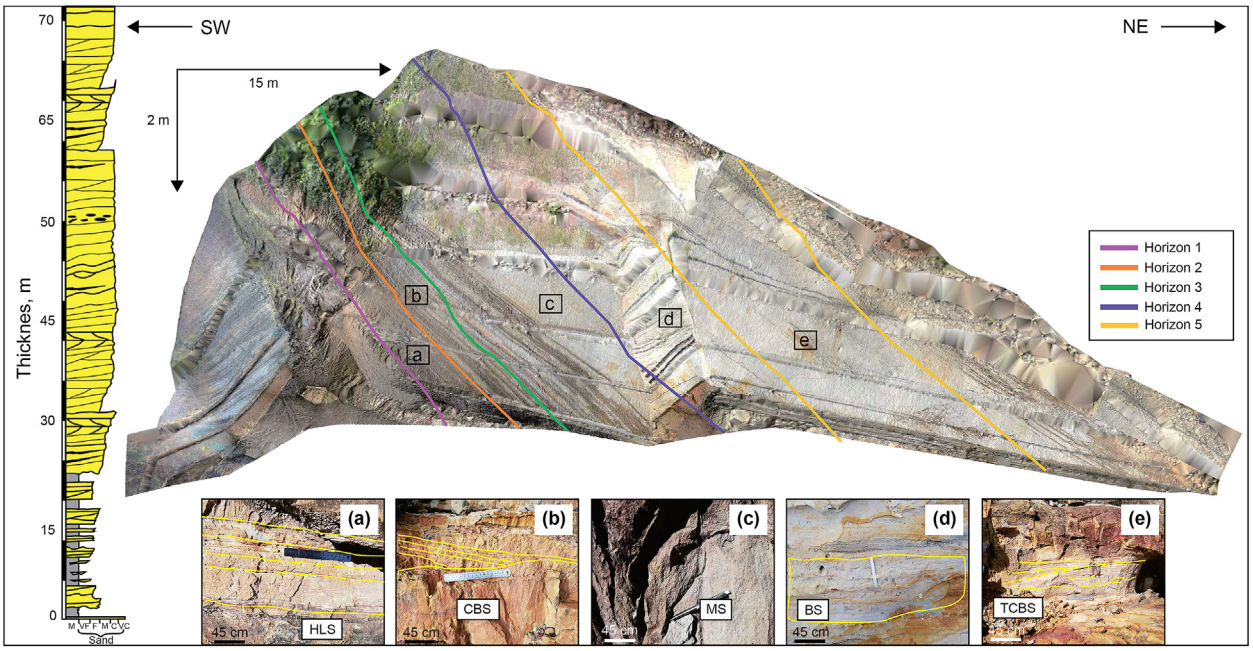

Fig. 5. VRGS view of VOM is showing the interpretation of the lithofacies with all real field data. The figure shows the interpreted horizons with different colors and closeup views show the sedimentary structures (PLS, CBS, MS, BS, TCBS) that formed in the interpreted lithofacies (a–e). The digitized lithofacies in VRGS with the sedimentary logs and virtual scales were used to measure the thickness and lateral heterogeneity in the measured section. On the left side, the real automatically generated georeferenced sedimentary log with actual grain size, lithology, bed thickness, facies association, and sedimentary structures with different colors.

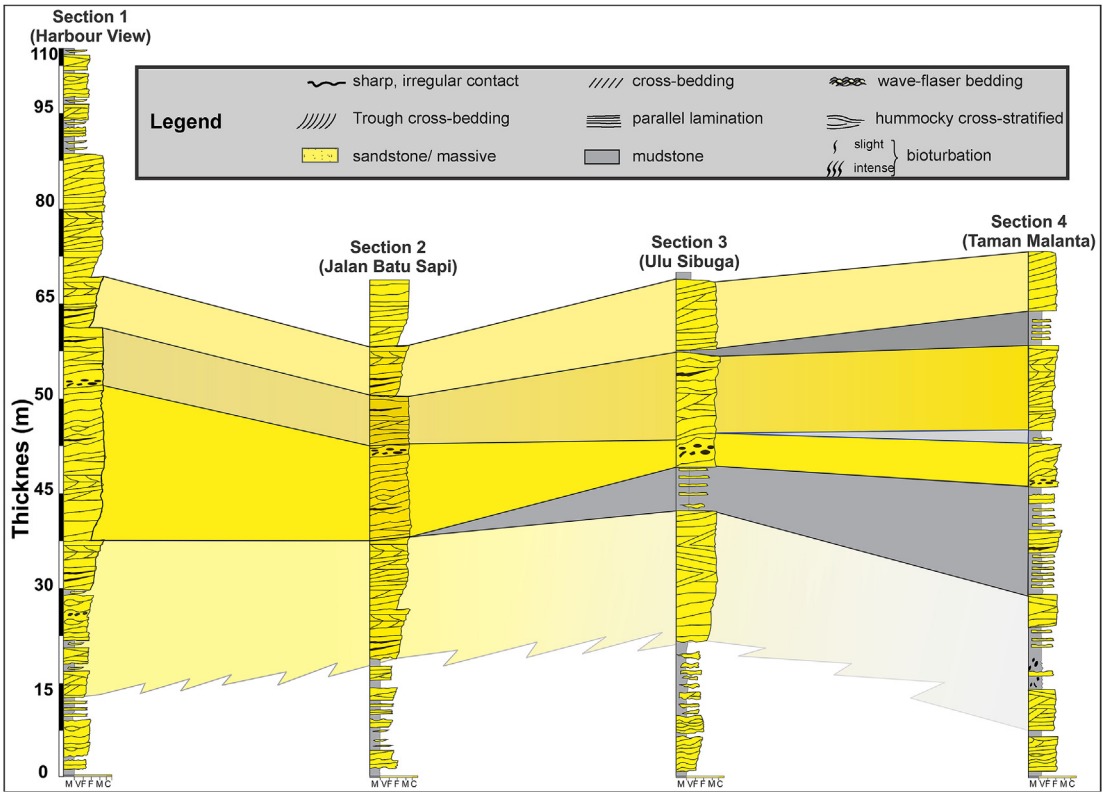

Fig. 6. Pseudo wells for the lateral and vertical distribution of all sandstone lithofacies correlation from LiDAR based scanned survey outcrop sections.

Pringle et al. (2006) to gain facies-based 3D geo-cellular model (Fig. 7) for the generation of petrophysical model to improve the understanding of lithofacies with reservoir flow simulation. Once all the input dataset has populated, we need the porosity and permeability ranges for all lithofacies in 3D geo-cellular model that has been discussed in detail as Section 3.4. According to the

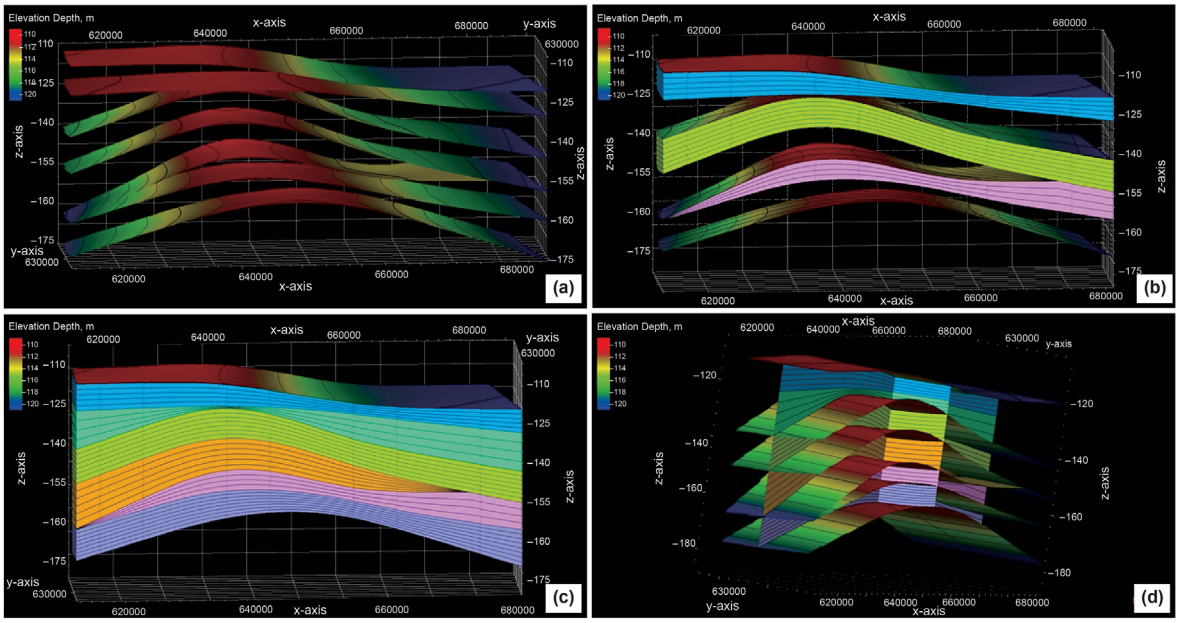

Fig. 7. 3D geo-cellular model. (a) 3D views of the interpreted horizons that are showing the subsurface structures with vertical and horizontal extrapolations. (b) sub horizons (zonation) of the stratigraphic key horizons and layering zonation with thickness and thinning. (c) six stratigraphic horizons with their sub-horizons which vary from 3 to 6 layers and depended upon the thickness of the lithofacies to mark thin beds. (d) cross-sectional view of the horizons and sub-horizons with the six stratigraphic surfaces.

quantitative analysis of porosity and permeability in the geo-modeling, the good reservoir lithofacies are CBS because these lithofacies have higher porosity and permeability ranging from 25.6% 16.8% and 74.03 mD to 66.84 mD. Fair reservoir is PLS because it has very good porosity (27.0%–20.2%) but low permeability (9.08 mD to 12.83 mD). BS lithofacies is very common but has poor reservoir quality as compare to PLS. It has good porosity (15.5%–18.6%) with low permeability (19.10 mD to 21.01 mD), because it is rich in mud matrix that mostly affects the connectivity of pores as permeability. Details of other lithofacies (variations and their continuity with the lateral extension that interpreted in the Virtual Reality Geological Studio (VRGS)) and reservoir properties are listed in Table 1.

4.4. 3D geo-cellular model for spatial distribution of lithofacies

3D geo-cellular model was obtained from all the input dataset (pseudo wells, point sets (*X, Y, Z* format) of interpreted horizons) in the Petrel™. For the zonation of the geo-cellular model, lithofacies information in the pseudo logs was upscaled according to the thickness to show the thin beds within the same lithofacies model (Fig. 7b and c). The object-based technique in the modelling software was used to illustrate the shape and dimensions of input parameters (Table 1) for 3D geo-cellular facies model (Deutsch and Wang, 1996; Deutsch and Tran, 2002; Falivene et al., 2007; Fabuel-Perez et al., 2010). 3D geo-cellular lithofacies model was interpolated and extrapolated in Petrel™, according to coordinates of the study area and interpreted key surfaces respectively (Fig. 7). Each lithofacies was modeled individually in the geo-cellular model to show the architecture of each horizon that was identified from the field study of Siddiqui et al. (2019). Lateral and vertical dimensions of massive to weak laminae sandstone (MWLS) lithofacies were easy to mark in the geo-cellular model (Fig. 7b, c, d) but were-difficult in the numerical analysis of 2D lithofacies connectivity (Siddiqui et al., 2019). Other two (2) lithofacies, cross-bedded sandstone (CBS) and parallel laminated sandstone (PLS) were also modeled with input parameters from Table 1 and Siddiqui et al. (2019) that showed the progradational paleoenvironment of the Sandakan sub-basin. The associations of all lithofacies were taken from upscaled pseudo wells/logs to interpret the thin bedded within the same lithofacies zonation (layering) technique used in the modeling software (Fig. 7).

4.5. Petrophysical modeling for 3D geo-models

Petrophysical model was completed through the stochastic algorithm that is Sequential Indicator Simulation (SISim) in the Petrel™ for resultant 3D geo-model to know the reservoir heterogeneity for each lithofacies (Fig. 8). SIS algorithm has applied by many researchers on different depositional system as fluvial, deltaic, aeolian and also on turbidites because in this algorithm facies hierarchy is not considerable for 3D geo-modeling (Langlais et al., 1993; Journel et al., 1998; Seifert and Jensen, 2000; Falivene et al., 2007). SIS algorithm works on transition probability of geo-statistics by Falivene et al. (2007) that provide transition probability location for lithofacies in a location. Petrophysical modeling includes porosity and permeability flow models for each lithofacies with key horizons and their sub-horizons (thin beds) to demonstrate the 3D petrophysical characteristics and heterogeneities in the thin beds (Fig. 8a and b). Simulated geo-model of three (3) lithofacies; cross-bedded sandstone (CBS), parallel laminated sandstone (PLS) and massive to weak laminae sandstone (MWLS) shows good to fair reservoir quality because of good porosity and permeability ranging from 27.01% to 20.2% and 74.03 mD to 9.08 mD respectively (Fig. 8a and b). After petrophysical properties of thin bedded reservoir media, the heterogeneity of porosity in all lithofacies is 21%–34% and the heterogeneity of permeability range is 8 mD to 90 mD. The cross-bedded sandstone (CBS) lithofacies

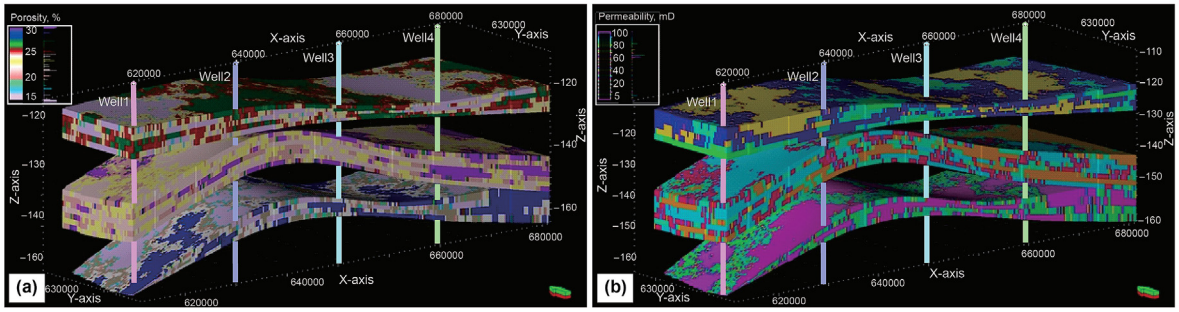

Fig. 8. 3D reservoir geo-modeling with heterogeneity of porosity and permeability in flow simulation model with pseudo wells different colors. (a) three-dimensional (3D) model according to the porosity and cross-bedded sandstone (CBS) has intense porosity variations. (b) three-dimensional (3D) model according to the heterogeneity of permeability in different lithofacies.

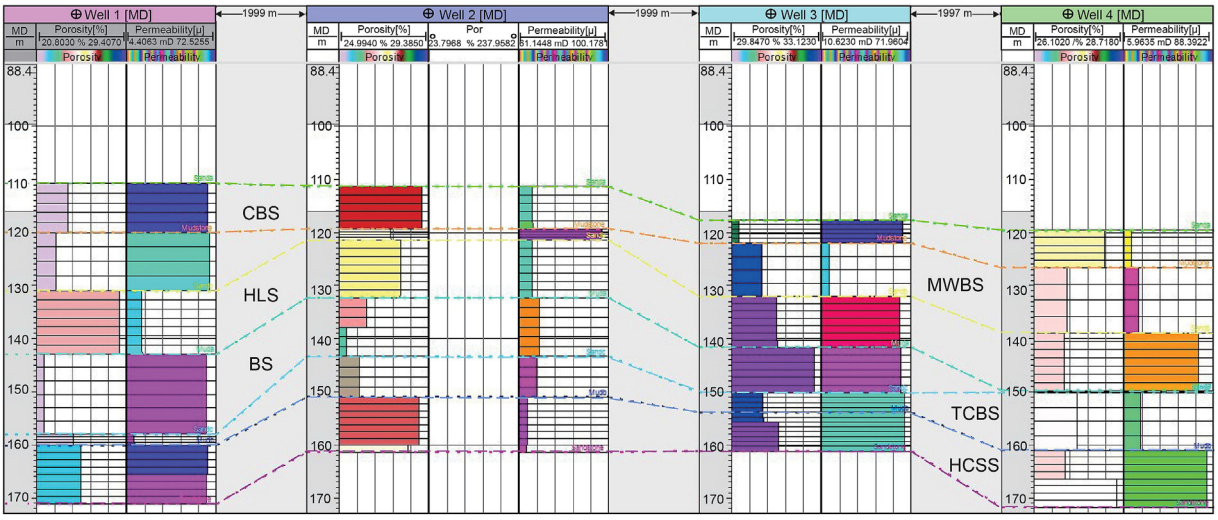

Fig. 9. Pseudo wells with the petrophysical modeling in all marked lithofacies with horizons that bound with the lateral continuity of lithofacies with different color codes in the model.

shows intense heterogeneity in the simulated 3D geo-model due to clay laminae with bioclasts of mud that was observed in the field survey.

4.6. Analysis of 3D model

The analysis of 3D model describes the distribution and association of the lithofacies with outcrop architecture to demonstrate the reservoir horizons with the petrophysical heterogeneities in the reservoir model (Figs. 8 and 9). In the 3D model, all sand rich lithofacies as cross-bedded sandstone (CBS), parallel laminated sandstone (PLS), and massive to weak laminae sandstone (MWLS) are good reservoir facies but other mud related lithofacies are non/poor reservoir facies. Based on this reservoir scheme, it has been elucidated that 3D spatial variations of petrophysical properties in the good reservoir facies are high in the 3D geo-cellular model (Fig. 7). Visual analysis in the well logs based petrophysical 2D model (Fig. 9) shows good to poor reservoir potential in the reservoir facies connectivity. With the help of connectivity parameter in 3D model, the same color grid cells define good reservoir facies as a thin bed within the same lithofacies. Mud related lithofacies shows baffling and barriers in reservoir connectivity because it is difficult to mark thin beds that have large amount of variations in porosity and permeability and no lateral continuity of facies in the spatial 3D model of the study area.

5. Discussions

5.1. VOMs and pseudo wells dataset in geo-modeling

Field based detailed studies of outcrop sections for lithofacies variations with the enhancement of geostatistical and analogue dataset reduce the uncertainties in the modeling (Narayanan et al., 1999; Pringle et al., 2006; Enge et al., 2007; Siddiqui et al., 2019). LiDAR based digital and virtual modeling of outcrops (VOMs) provide highly geospatial input dataset that reduces the uncertainties from 10's of km to cm (Enge et al., 2007; Rarity et al., 2014). That can be used for the industry with the integration of seismic and pseudo well logs in the modeling software by filling up the resolution scale between VOMs and conventional geophysical data (Brandsæter et al., 2005; Jackson et al., 2005; Coburn et al., 2006; Fabuel-Perez et al., 2009b; 2010; Rarity et al., 2014; Siddiqui et al., 2019). In this study, the digitized outcrops and pseudo well logs (Figs. 5 and 6) were used to integrate the petrophysical lithofacies model in the Petrel™ to demonstrate the reservoir heterogeneity with respect to porosity and permeability in thin beds (Fig. 7). The input dataset for this modeling covers all geological characteristics and also maintained for long outcrops as Pringle et al. (2006); Fabuel-Perez et al. (2009b, 2010); Rarity et al. (2014); Siddiqui et al. (2019). We have used VRGS software for 3D interpretation of the geostatistical dataset including key horizons and pseudo wells

according to Løseth et al. (2004); Wilson et al. (2009); Enge et al. (2007); Fabuel-Perez et al. (2010); Rarity et al. (2014), to generate three-dimensional models. In the 3D geo-cellular and petrophysical well logs model (Figs. 7c, 8, 9), the association and distributions of the lithofacies correspond to the VOM of the study that shows high precision of the dataset and it has been discussed by many researchers in their studies of the VOMs of sandstone facies architecture (Fabuel-Perez et al., 2009b, 2010; Rarity et al., 2014; Howell et al., 2014; Newell and Shariatipour, 2016; Seers, 2017; Siddiqui et al., 2019).

The most important contribution in the study is the spatial elucidation of thin beds in the 3D geo-model for the petrophysical characteristics and heterogeneities. Previous studies were only done just for the 2D connectivity of thin beds with the static model (Siddiqui et al., 2019). For better understanding and elucidation, object-based technique was used for each lithofacies to improve the shape and dimensions of LiDAR based input dataset for all lithofacies (Deutsch and Wang, 1996; Deutsch and Tran, 2002; Falivene et al., 2007; Fabuel-Perez et al., 2010; Siddiqui et al., 2019). According to the 3D geo-model, sandstone rich facies (CBS, PLS, MWLS) are overall good reservoir due to high porosity and permeability from 27.01% to 20.2% and 74.03 mD to 9.08 mD, respectively, whereas mudstone rich facies are non or poor reservoir facies (Fig. 8a and b, 9). The accuracy of the 3D geo-model for petrophysical properties has described an individual parameter on the basis of net to non-net reservoir facies. HCSS and MWLS reservoir facies are extensively appeared that have good reservoir quality in both studies that are LiDAR based VOMs and, in the 3D geo-model (Figs. 5, 8a and 8b). MWLS, TCBS and BS reservoir facies are also present but their modeled lithofacies laterally and vertically are not well developed and are low quality reservoirs due to the presences of the mud baffles or barriers within thin beds. These variations of thin beds within all lithofacies are the main responsible agent for the continuity or discontinuity of high permeability that is elucidating the reservoir heterogeneity in terms of 3D petrophysical model.

5.2. Uncertainties and limitations of input analogue dataset

This work was done to improve the applications of the input analogue dataset of outcrops with the help of virtual outcrop modeling (VOM) based on VRGS software. We followed the workflow of previous researchers (Fabuel-Perez et al., 2009b; 2010; Rarity et al., 2014; Howell et al., 2014) in addition to extemporizing the experimental petrophysical (porosity and permeability) values in the industry-based reservoir modeling software Petrel™ with geostatistical dataset. The VOMs dataset help to reduce the uncertainties in the surface-based 3D geo-cellular and petrophysical modeling of the reservoir facies (Fabuel-Perez et al., 2009b; 2010; Rarity et al., 2014). But still, there are main uncertainties in the extrapolation of input dataset of 3D geo-modeling as 3D gridding cells with petrophysical properties that have been described.

Uncertainties related to input dataset and limitations: interpretation of the VOMs analogues is tenuous work (Fabuel-Perez et al., 2009b, 2010; Howell et al., 2014; Rarity et al., 2014; Siddiqui et al., 2019) to deal with, we scanned 3 outcrop sections to get enough data and do the interpretation for lateral and vertical extension of the lithofacies VRGS software used according to Fabuel-Perez et al. (2010). Still, there is a limitation of the scanned dataset for the 3D geo-modeling to describe the subsurface reservoir heterogeneities. Uncertainties of 3D geo-modeling for the laterally and vertical spatial distribution of the reservoir facies, Petrel™ software provides enough illustration but still some ambiguities and complexities remain in the final model as gridding cells (Fabuel-Perez et al., 2010; Rarity et al., 2014; Newell and Shariatipour, 2016; Seers, 2017), to deal with this, we interpret the key horizons, pseudo wells, and zonation with enough gridding cells in geo-cellular model of all lithofacies to ensure the 3D geo-model requirements.

6. Conclusions

The integrated studies of the surface-based geostatistical analogues and field sedimentary data give a procedure of the interpretation for the reservoir properties and heterogeneities in petrophysical modeling on Sandakan Formation, NW, Borneo. The geostatistical data of the VOMs shows the propagation of the key horizons (stratigraphic surfaces) and their sub horizons (zonation) for 3D geo-cellular modeling of lithofacies in the Petrel™ suite. This integration of VOMs dataset for the 3D geo-cellular modeling with the reservoir properties allows to elucidate the subsurface modeling based on the high-resolution sedimentological dataset. The reservoir properties of the 3D modeled lithofacies in the Petrel™ software show that CBS, PLS and MWLS have good to fair reservoir quality with heterogenous porosity and permeability from 27.0% to 20.2% and 74.03 mD to 9.08 mD, respectively. In the 3D geo-cellular and petrophysical model, other lithofacies have poor reservoir quality due to the high baffling of surrounding sediments of mudstone and sand particles, which was studied in the high-resolution dataset. This modeling study shows the 3D dynamic spatial connectivity of all lithofacies that were 2D in the outcrop sections. Based on reservoir properties in the 3D petrophysical model, there are strong heterogeneities of porosity and permeability in the Sandakan Formation that would influence the reservoir quality within the Sandakan sub-basin reservoirs. There are some uncertainties in the surface-based 3D reservoir modeling dataset that shows errors in the resultant 3D geo-cellular and petrophysical model that can be decreased by increasing the sample size of scanning positions and with the integration of subsurface dataset. This improvised high-resolution sedimentological study with the 3D geo-cellular model could be utilized to enhance the reservoir modeling in the petroleum industry.

Acknowledgment

Authors are thankful to the Cooperation Basement of International Science and Technology on Deep Reservoir-forming Mechanism, Qingdao, China University of Petroleum, and the Universiti Teknologi PETRONAS, Malaysia, for research collaboration agreement.

References

Madon, M., 1999. Sabah Basin. in the petroleum geology and resources of Malaysia 1, 499–542.

Adams, E.W., Grotzinger, J.P., Watters, W.A., et al., 2005. Digital characterization of thrombolite-stromatolite reef distribution in a carbonate ramp system (terminal Proterozoic, Nama Group, Namibia). AAPG Bull. 89 (10), 1293–1318. https://doi.org/10.1306/06160505005.

Ahmed, N., Siddiqui, N.A., Rahman, A.H., et al., 2021a. Evaluation of hydrocarbon source rock potential: deep marine shales of Belaga Formation of late Cretaceous-late Eocene, Sarawak, Malaysia. J. King Saud Univ. Sci. 33 (1), 101268. https://doi.org/10.1016/j.jksus.2020.101268.

Ahmed, N., Siddiqui, N.A., Ramasamy, N., et al., 2021b. Geochemistry of eocene bawang member turbidites of the belaga formation, Borneo: implications for provenance, palaeoweathering, and tectonic setting. Geol. J. 1–23. https://doi.org/10.1002/gj.4062.

Aigner, T., Braun, S., Palermo, D., et al., 2007. 3D geological modelling of a carbonate shoal complex: reservoir analogue study using outcrop data. First Break 25 (8). https://doi.org/10.3997/1365-2397.2007022.

Amour, F., Mutti, M., Christ, N., 2012. Capturing and modelling metre-scale spatial facies heterogeneity in a Jurassic ramp setting (Central High Atlas, Morocco). Sedim 59, 1158–1189. https://doi.org/10.1111/j.1365-3091.2011.01299.x.

Arbués, P., Mellere, D., Falivene, O., et al., 2007. Context and architecture of the ainsa-1-quarry channel complex, ainsa basin, eocene south-central pyrenees,

Spain. In: Nielsen, T.H., Shew, R.D., Steffens, G.S., Studlick, R.J. (Eds.), Atlas of Deep-Water Outcrops: AAPG Stud in Geol, 56. CD-ROM, p. 20. https://doi.org/10.1306/12401016St563310.
Azlina, A., Muhammad, A.J., 1995. Geochemical evaluation of Sandakan-Lahad Datu dent Peninsula areas, East Sabah, Malaysia. PETRONAS Report No. PRSS95-03 25–35.
Bastante, F.G., Ordóñez, C., Taboada, J., et al., 2008. Comparison of indicator kriging, conditional indicator simulation and multiple-point statistics used to model slate deposits. Eng. Geol. 98 (1-2), 50–59. https://doi.org/10.1016/j.enggeo.2008.01.006.
Bell, R.M., Jessop, R.G.C., 1974. Exploration and geology of the west Sulu basin, Philippines. The APPEA Jour 14 (1), 21–28. https://doi.org/10.1071/AJ73003.
Bellian, J.A., Kerans, C., Jennette, D.C., 2005. Digital outcrop models: applications of terrestrial scanning lidar technology in stratigraphic modeling. J Sed Res 75 (2), 166–176. https://doi.org/10.2110/jsr.2005.013.
Bellian, J.A., Beck, R., Kerans, C., 2007. Analysis of hyperspectral and lidar data: remote optical mineralogy and fracture identification. Geosph 3 (6), 491–500. https://doi.org/10.1130/GES00097.1.
Brandsæter, I., Mcilroy, D., Lia, O., et al., 2005. Reservoir modelling and simulation of Lajas Formation outcrops (Argentina) to constrain tidal reservoirs of the Halten Terrace (Norway). Petrol. Geosci. 11 (1), 37–46. https://doi.org/10.1144/1354-079303-611.
Brush, J.A., Pavlis, T.L., Hurtado, J.M., et al., 2019. Evaluation of field methods for 3-D mapping and 3-D visualization of complex metamorphic structure using multiview stereo terrain models from ground-based photography. Geosph 15 (1), 188–221. https://doi.org/10.1130/GES01691.1.
Bryant, I.D., Carr, D.P., Cirilli, N., et al., 2000. Use of 3D digital analogues as templates in reservoir modelling. Petrol. Geosci. 6 (2), 195–201. https://doi.org/10.1144/petgeo.6.2.195.
Buckley, S.J., Howell, J., Enge, H., Kurz, T., 2008. Terrestrial laser scanning in geology: data acquisition, processing and accuracy considerations. J of the Geol Soc 165 (3), 625–638. https://doi.org/10.1144/0016-76492007-100.
Buckley, B., Naumann, S.J., Kurz, N.K., Eide, C.H., 2016. In: 2nd Virtual Geoscience Conference, Proceedings Volume. Uni Research CIPR, Bergen, Norway, p. 212.
Charles, K., 1999. Stratigraphic correlation surfaces and 3D reservoir model construction: constraints from walther's law models and outcrop analogue data. In: GCSSEPM Foundation 19th Annual Research Conference. The Univ of Texas at Austin, pp. 105–111.
Clennell, M.B., 1996. Far-field and gravity tectonics in Miocene basins of Sabah, Malaysia. In: Hall, R., Blundell, D. (Eds.), Tectonic Evolution of Southeast Asia, 106. Geol Soc of London Spec Pub, pp. 307–320. https://doi.org/10.1144/GSL.SP.1996.106.01.20.
Coburn, T.C., Yarus, J.M., Chambers, R.L., 2006. Geostatistics and stochastic modeling: bridging into the 21st century. In: Coburn, T.C., Yarus, J.M., Chambers, R.L. (Eds.), Stochastic Modeling and Geostatistics: Principles, Methods, and Case Studies, Volume II, 5. AAPG Comp. Appl. Geol., pp. 3–9. https://doi.org/10.1306/10631037CA51306
Collenette, P., 1965. The geology and mineral resources of the pensiangan and upper Kinabatangan area, Sabah, Malaysia Geol. Survey Malaysia, Borneo Region. Memoir 12, 150.
Collenette, P., 1966. The Garinono formation, Sabah, Malaysia. Borneo Region Mal Geol Surv Ann Rep 161–167.
De Paor, D., 2016. Virtual Rocks. GSA Today (Geol. Soc. Am.) 26 (8), 4–11. https://doi.org/10.1130/GSATG257A.1.
Deutsch, C.V., Tran, T.T., 2002. FLUVSIM: a program for object-based stochastic modeling of fluvial depositional systems. Comp. & Geosci. 28 (4), 525–535. https://doi.org/10.1016/S0098-3004(01)00075-9.
Deutsch, C.V., Wang, L., 1996. Hierarchical object-based stochastic modelling of fluvial reservoirs. Math. Geol. 28 (7), 851–880. https://doi.org/10.1007/BF02066005.
Eaton, T.T., 2006. On the importance of geological heterogeneity for flow simulation. Sed Geol 184 (3-4), 187–201. https://doi.org/10.1016/j.sedgeo.2005.11.002.
Enge, H.D., Buckley, S.J., Rotevatn, A., et al., 2007. From outcrop to reservoir simulation model: workflow and procedures. Geosph 3 (6), 469–490. https://doi.org/10.1130/GES00099.1.
Fabuel-Perez, I., Hodgetts, D., Redfern, J., 2009. A new approach for outcrop characterization and geostatistical analysis of a low-sinuosity fluvial-dominated succession using digital outcrop models: Upper Triassic Oukaimeden Sandstone Formation, central High Atlas, Morocco. Amer Assoc of Pet Geol Bull 93 (6), 795–827. https://doi.org/10.1306/02230908102.
Fabuel-Perez, I., Hodgetts, D., Redfern, J., 2010. Integration of digital outcrop models (DOMs) and high-resolution sedimentology workflow and implications for geological modelling: Oukaimeden Sandstone Formation, High Atlas (Morocco). Pet Geos 16 (2), 133–154. https://doi.org/10.1144/1354-079309-820.
Falivene, O., Arbués, P., Gardiner, A., 2006. Best practice stochastic facies modeling from a channel-fill turbidite sandstone analog (the Quarry outcrop, Eocene Ainsa basin, northeast Spain). AAPG (Am. Assoc. Pet. Geol.) Bull. 90 (7), 1003–1029. https://doi.org/10.1306/02070605112.
Falivene, O., Cabrera, L., Muñoz, J., et al., 2007. Statistical grid-based facies reconstruction and modelling for sedimentary bodies. Alluvial-palustrine and turbiditic examples. Geol. Acta 5 (3), 199–230.
Fei, J., Yarus, J., Chambers, R., 2016. Data mining methodologies to reduce the uncertainty of reservoir selection. In: AAPG Ann Conv and Exhib.
Franke, D., Savva, D., Pubellier, M., et al., 2014. The final rifting evolution in the South China Sea. Mar. Petrol. Geol. 58, 704–720. https://doi.org/10.1016/j.marpetgeo.2013.11.020.
Futalan, K., Mitchell, A., Amos, K., Backe, G., 2012. Seismic facies analysis and structural interpretation of the Sandakan sub-basin, Sulu Sea, Philippines. AAPG Search and Discovery 30254.
Gold, P.O., Cowgill, E., Kreylos, O., et al., 2012. Terrestrial lidar-based workflow for determining three–dimensional slip vectors and associated uncertainties. Geosph 8 (2), 431–442. https://doi.org/10.1130/GES00714.1.
Gomes, J., Parra, H., Ghosh, D., 2018. Quality Control of 3D GeoCellular models: Examples from UAE Carbonate Reservoirs. In: Abu Dhabi Int Pet Exhib & Conf. https://doi.org/10.2118/193128-MS.
Gotway, C.A., Rutherford, B.M., 1994. Stochastic simulation for imaging spatial uncertainty: Comparison and evaluation of available algorithms. In: Armstrong, M., Dowd, P.A. (Eds.), Geostatistical Simulation, 7. Kluwer Acad., Dordrecht, pp. 1–22. https://doi.org/10.1007/978-94-015-8267-4_1.
Graves, J.E., Swauger, D.A., 1997. Petroleum systems of the Sandakan basin, Philippines. In: Proceedings of an International Conference on Petroleum Systems of SE Asia and Australasia, pp. 21–23. Jakarta.
Hall, R., 2002. Cenozoic geological and plate tectonic evolution of SE Asia and the SW Pacific: computer-based reconstructions, model and animations. J. Asian Earth Sci. 20 (4), 353–431. https://doi.org/10.1016/S1367-9120(01)00069-4.
Hall, R., 2013. Contraction and extension in northern Borneo driven by subduction rollback. J. Asian Earth Sci. 76, 399–411. https://doi.org/10.1016/j.jseaes.2013.04.010.
Henriquez, A., Jourdan, C., 1995. Challenges in modelling reservoirs in the north Sea and on the Norwegian shelf. Petrol. Geosci. 1, 327–336. https://doi.org/10.1144/petgeo.1.4.327.
Howell, J.A., Martinius, A.W., Good, T.R., 2014. The application of outcrop analogues in geological modelling: a review, present status and future outlook. Geol Soc of London Spec Pub 387 (1), 1–25. https://doi.org/10.1144/SP387.12.
Hutchison, C.S., 2005. Geology of North-West Borneo: Sarawak. Elsevier, Brunei and Sabah, pp. 175–177.
Immenhauser, A., Hillgartner, H., Sattler, U., et al., 2004. Barremian-lower Aptian Qishn Formation, Haushi-Huqf area, Oman: a new outcrop analogue for the Kharaib/Shu'aiba reservoirs. GeoArabia 9 (1), 153–194.
Jackson, M., Yoshida, S., Muggeridge, A., et al., 2005. Three-dimensional reservoir characterization and flow simulation of heterolithic tidal sandstones. AAPG Bull. 89 (4), 507–528. https://doi.org/10.1306/11230404036.
Jamil, M., Rahman, A.H.A., Siddiqui, N.A., et al., 2020. A contemporary review of sedimentological and stratigraphic framework of the Late Paleogene deep marine sedimentary successions of West Sabah, North-West Borneo. Bull of the Geo Soc of Mal 69, 53–65. https://doi.org/10.7186/bgsm69202005.
Jones, R.R., Wawrzyniec, T.F., Holliman, N.S., et al., 2008. Describing the dimensionality of geospatial data in the earth sciences Recommendations for nomenclature. Geosphere 4 (2), 354–359. https://doi.org/10.1130/GES00158.1.
Journel, A.G., Gundeso, R., Gringarten, E., et al., 1998. Stochastic modelling of a fluvial reservoir: a comparative review of algorithms. J. Petrol. Sci. Eng. 21 (1-2), 95–121. https://doi.org/10.1016/S0920-4105(98)00044-8.
Kjønsvik, D., Doyle, J., Jacobsen, T., et al., 1994. The effects of sedimentary heterogeneities on production from a shallow marine Reservoir - what Really matters? SPE 28445, 27–40. https://doi.org/10.2118/28445-MS.
Koehrer, B.S., Heymann, C., Prousa, F., et al., 2010. Multi-scale facies and reservoir quality variations within a dolomite body – outcrop analog study from the Middle Triassic, SW German Basin. Mar. Petrol. Geol. 27 (2), 386–411. https://doi.org/10.1016/j.marpetgeo.2009.09.009.
Kurz, T.H., Buckley, S.J., Howell, J.A., et al., 2011. Integration of panoramic hyperspectral imaging with terrestrial lidar data. The Photogram. Rec. 26 (134), 212–228. https://doi.org/10.1111/j.1477-9730.2011.00632.x.
Langlais, V., Doyle, J.D., Sweet, M.L., et al., 1993. An additional geological input to the sequential indicator simulation (S.I.S.): the vertical organization of lithofacies. In: Eschard, R., Doliguez, B.E. (Eds.), Subsurface Reservoir Characterization from Outcrop Observations. Éditions Technip, Paris, pp. 111–123.
Lee, D.T.C., 1970. Sandakan Peninsula, Eastern Sabah, East Malaysia. US Government Printing Office, pp. 45–77.
Løseth, T., Rivenaes, J.C., Thurmond, J.B., et al., 2004. The value of digital outcrop data in reservoir modeling. In: AAPG Conf., pp. 16–23. USA.
Mathew, M.J., Siddiqui, N.A., Menier, D., 2014. An evolutionary model of the Nearshore Tinjar and balingian provinces, Sarawak, Malaysia. Int. J. Petrol. Geosci. Eng. 1 (2), 81–91.
Mathew, M.J., Menier, D., Siddiqui, N., Ramkumar, M., et al., 2016b. Drainage basin and topographic analysis of a tropical landscape: insights into surface and tectonic processes in northern Borneo. J. Asian Earth Sci. 124, 14–27. https://doi.org/10.1016/j.jseaes.2016.04.016.
Mathew, M.J., Menier, D., Siddiqui, N.A., Kumar, S.G., et al., 2016a. Active tectonic deformation along rejuvenated faults in tropical Borneo: inferences obtained from tectono-geomorphic evaluation. Geomorph 267, 1–15. https://doi.org/10.1016/j.geomorph.2016.05.016.
Menier, D., Mathew, M., Pubellier, M., et al., 2017. Landscape response to progressive tectonic and climatic forcing in NW Borneo: implications for geological and geomorphic controls on flood hazard. Sci. Rep. 7 (1), 1–18. https://doi.org/10.1038/s41598-017-00620-y.
Mikes, D., Geel, C.R., 2006. Standard facies models to incorporate all heterogeneity levels in a reservoir model. Mar. Petrol. Geol. 23 (9-10), 943–959. https://doi.org/10.1016/j.marpetgeo.2005.06.007.
Narayanan, K., White, C.D., Lake, L.W., Willis, B.J., 1999. Response surface methods for upscaling heterogeneous geologic models. In: Proceedings of 15th

Symposium on Reservoir Simulation, 2, pp. 30–57. https://doi.org/10.2118/51923-MS.
Newell, A.J., Shariatipour, S.M., 2016. Linking outcrop analogue with flow simulation to reduce uncertainty in sub-surface carbon capture and storage: an example from the Sherwood Sandstone Group of the Wessex Basin, UK. Geol Soc London, Special Pub. 436 (1), 231–246. https://doi.org/10.1144/SP436.2.
Notebaert, B., Verstraeten, G., Govers, G., et al., 2009. Qualitative and quantitative applications of LiDAR imagery in fluvial geomorphology. Earth Surf. Process. Landforms 34, 217–231. https://doi.org/10.1002/esp.1705.
Palermo, D., Aigner, T., Nardon, N., et al., 2010. Three-dimensional facies modeling of carbonate sand bodies: outcrop analog study in an epicontinental basin (Triassic, southwest Germany). AAPG Bull. 94 (4), 475–512. https://doi.org/10.1306/08180908168.
Pavlis, T.L., Bruhn, R.L., 2011. Application of LIDAR to resolving bedrock structure in areas of poor exposure: an example from the STEEP study area, southern Alaska. Geol Soc of Amer Bull 123 (1-2), 206–217. https://doi.org/10.1130/B30132.1.
Pavlis, T.L., Mason, K.A., 2017. The new world of 3D geologic mapping. GSA Today (Geol. Soc. Am.) 27 (9), 4–10. https://doi.org/10.1130/GSATG313A.1.
Phelps, R.M., Kerans, C., Scott, S.Z., et al., 2008. Three-dimensional modelling and sequence stratigraphy of a carbonate ramp-to-shelf transition, Permian Upper San Andres Formation. Sedim 55 (6), 1777–1813. https://doi.org/10.1111/j.1365-3091.2008.00967.x.
Pranter, M.J., Ellison, A.I., Cole, R.D., et al., 2007. Analysis and, modeling of intermediate-scale reservoir heterogeneity based on a fluvial point-bar outcrop analog, Williams Fork Formation, Piceance Basin, Colorado. AAPG Bull. 91 (7), 1025–1051. https://doi.org/10.1306/02010706102.
Pringle, J.K., Howell, J.A., Hodgetts, D., et al., 2006. Virtual outcrop models of petroleum reservoir analogues: a review of the current state-of-the-art. First Break 24 (3), 33–42. https://doi.org/10.3997/1365-2397.2006005.
Qi, L., Car, T.R., Goldstein, R.H., 2007. Geostatistical three-dimensional modeling of oolite shoals, St. Louis Limestone, southwest Kansas. AAPG Bull. 91 (1), 69–96. https://doi.org/10.1306/08090605167.
Ramkumar, M., Santosh, M., Nagarajan, R., et al., 2018. Late middle Miocene volcanism in northwest Borneo, Southeast asia: implications for tectonics, paleoclimate and stratigraphic marker. Palaeogeo, Palaeocli Palaeoeco. 490, 141–162. https://doi.org/10.1016/j.palaeo.2017.10.022.
Rangin, C., Bellon, H., Benard, F., et al., 1990. Neogene arc-continent collision in Sabah, northern Borneo (Malaysia). Tectonophysics 183, 305–319. https://doi.org/10.1016/0040-1951(90)90423-6.
Rarity, F., Van Lanen, X.M.T., Hodgetts, D., et al., 2014. LiDAR-based digital outcrops for sedimentological analysis: workflows and techniques. Geol Society, London, Spec Pub. 387 (1), 153–183. https://doi.org/10.1144/SP387.5.
Redfern, J., Hodgetts, D., Fabuel-Perez, I., 2007. Digital analysis brings renaissance for petroleum geology outcrop studies in North Africa. First Break 25 (2), 81–87. https://doi.org/10.3997/1365-2397.25.1104.27337.
Sapin, F., Pubellier, M., Lahfid, A., et al., 2011. Onshore record of the subduction of a crustal salient: example of the NW Borneo Wedge. Terra. Nova 23 (4), 232–240. https://doi.org/10.1111/j.1365-3121.2011.01004.x.
Seers, T.D.S., Hodgetts, D.H., Wang, Y.W., Fadlelmula, M.F., 2017. Direct computation of fracture network equivalent porous medium properties using digital outcrop models. 79th EAGE Conf and Exhib 1, 1–5. https://doi.org/10.3997/2214-4609.201700647.
Seifert, D., Jensen, J.L., 2000. Object and pixel-based reservoir modeling of a braided fluvial reservoir. Math. Geol. 32 (5), 581–603. https://doi.org/10.1023/A:1007562221431.
Shepherd, M., 2009. 3-D geocellular modeling. In: Shepherd, M. (Ed.), Oil Field Production Geology. AAPG Mem, 91, pp. 175–188.
Siddiqui, N.A., Ramkumar, M., Rahman, A.H.A., et al., 2019. High resolution facies architecture and digital outcrop modeling of the Sandakan formation sandstone reservoir, Borneo: implications for reservoir characterization and flow simulation. Geosci Front 10 (3), 957–971. https://doi.org/10.1016/j.gsf.2018.04.008.
Siddiqui, N.A., Mathew, M.J., Ramkumar, M., et al., 2020. Sedimentological characterization, petrophysical properties and reservoir quality assessment of the onshore Sandakan Formation, Borneo. J. Petrol. Sci. Eng. 186, 106771. https://doi.org/10.1016/j.petrol.2019.106771.
Sima, A.A., 2013. An improved workflow for image-and laser-based virtual geological outcrop modelling. Univ. of Bergen. PhD Thesis. 24–67.
Slob, S., Hack, R., 2004. 3D terrestrial laser scanning and a new field measurement and monitoring technique. In: Hack, R., Azzam, R., Charlier, R. (Eds.), Engineering Geology for Infrastructure Planning: A European Perspective. Lect Notes in Earth Sci, 104, pp. 179–189. https://doi.org/10.1007/978-3-540-39918-6_22.
Stauffer, P.H., Lee, D.T.C., 1972. Sedimentology of the Sandakan Formation, East Sabah. Geol Surv of Mal 1, 10–17.
Tinker, S.W., 1996. Building the 3-D jigsaw puzzle: applications of sequence stratigraphy to 3-D reservoir characterization, Permian basin. AAPG Bull. 80 (4), 460–485. https://doi.org/10.1306/64ED8818-1724-11D7-8645000102C1865D.
Tjia, H.D., Komoo, I., Lim, P.S., Surat, T., 1990. The Maliau basin, Sabah: geology and tectonic setting. Bull of the Geol Soc of Mal 27, 261–292. https://doi.org/10.7186/bgsm27199013.
Tolosana-delgado, R., Pawlowsky-Glahn, V., Egozcue, J.-J., 2008. Indicator kriging without order Relation violations. Math. Geosci. 40, 327–347. https://doi.org/10.1007/s11004-008-9146-8.
Tomàs, S., Zitzmann, M., Homann, M., et al., 2010. From ramp to platform: building a 3D model of depositional geometries and facies architectures in transitional carbonates in the Miocene, northern Sardinia. Facies 56, 195–210. https://doi.org/10.1007/s10347-009-0203-7.
Usman, M., Siddiqui, N.A., Zhang, S., et al., 2020a. Ichnofacies and sedimentary structures: a passive relationship with permeability of a sandstone reservoir from NW Borneo. J. Asian Earth Sci. 192, 103992. https://doi.org/10.1016/j.jseaes.2019.103992.
Usman, M., Zhang, S., Siddiqui, N.A., et al., 2020b. The influential parameters of the reservoir quality of Sandakan sandstone, NW Borneo. In: 2nd SEG Rock Physics Workshop: Challenges in Deep and Unconventional Oil/Gas Exploration. Soc of Exp Geophys, pp. 8–11. https://doi.org/10.1190/rpwk2019-007.1.
Usman, M, Siddiqui, NA., Garzanti, E, et al., 2021. 3-D Seismic-based Upper Jurassic to Lower Cretaceous stratigraphic and structural interpretation of the Gullfaks Field, Norwegian North Sea: A case study of reservoir development. Ener Geo. https://doi.org/10.1016/j.engeos.2021.06.001.
Usman, M., Siddiqui, N.A., Mathew, M., et al., 2020c. Linking the influence of diagenetic properties and clay texture on reservoir quality in sandstones from NW Borneo. Mar. Petrol. Geol. 120, 104509. https://doi.org/10.1016/j.marpetgeo.2020.104509.
Verwer, K., Merino-tome, O., Kenter, J.A., et al., 2009. Evolution of a high-relief carbonate platform slopeusing 3D digital outcrop models: lower Jurassic Djebel bou Dahar, high atlas, Morocco. J. Sed. Res. 79 (6), 416–439. https://doi.org/10.2110/jsr.2009.045.
Westoby, M.J., Brasington, J., Glasser, N.F., et al., 2012. Structure-from-Motion' photogrammetry: a low-cost, effective tool for geoscience applications. Geomorph 179, 300–314. https://doi.org/10.1016/j.geomorph.2012.08.021.
White, C.D., Novakovic, D., Dutton, S.P., et al., 2003. A geostatistical model for Calcite Concretions in sandstone. Math. Geol. 35, 549–575. https://doi.org/10.1023/A:1026282602013.
Wilkinson, M.W., Jones, R.R., Woods, C.E., et al., 2016. A comparison of terrestrial laser scanning and structure-from-motion photogrammetry as methods for digital outcrop acquisition. Geosph 12 (6), 1865–1880. https://doi.org/10.1130/GES01342.1.
Wilson, R.A.M., 1961. The geology and mineral resources of the Banggi island and Sugut River area. North Borneo. British Borneo Geological Survey Memoir 15.
Wilson, P., Hodgetts, D., Rarity, F., et al., 2009. Structural geology and 4D evolution of a half-graben: new digital outcrop modelling techniques applied to the Nukhul half-graben, Suez rift, Egypt. J of Struc Geol 31 (3), 328–345. https://doi.org/10.1016/j.jsg.2008.11.013.
Xu, X., Aiken, C., Bhattacharya, J., et al., 2000. Creating virtual 3-D outcrop. Lead. Edge 19 (2), 197–202.
Yarus, J.M., Chambers, R.L., Maucec, M., et al., 2012. Facies simulation in practice: Lithotype proportion mapping and Plurigaussian simulation, a powerful combination. In: Paper P-014 Presented at the 9th Intel Geostat Cong Oslo, pp. 11–15. Nor.
Zappa, G., Bersezio, R., Felletti, F., et al., 2006. Modeling heterogeneity of gravel-sand, braided stream, alluvial aquifers at the facies scale. J of Hydrol 325, 134–153. https://doi.org/10.1016/j.jhydrol.2005.10.016.